A Comparative Study on Electrochemical Micromachining of n-GaAs and p-Si by Using Confined Etchant Layer Technique

Li Zhang,[†] Xin Z. Ma,[†] Mi X. Lin,[†] Yu Lin,[†] Guo H. Cao,*[,‡] Jing Tang,*[,†] and Zhao W. Tian[†]

Department of Chemistry, College of Chemistry and Chemical Engineering, Xiamen University, Xiamen, 361005, China, and Department of Mechanical Manufacture and Automation, Harbin Institute of Technology, Harbin, 150001, China

Received: May 22, 2006; In Final Form: July 21, 2006

The confined etchant layer technique has been applied to achieve effective three-dimensional (3D) micromachining on n-GaAs and p-Si. This technique operates via an indirect electrochemical process and is a maskless, low-cost technique for microfabrication of arbitrary 3D structures in a single step. Br_2 was electrogenerated at the mold surface and used as an efficient etchant for n-GaAs and p-Si; l-cystine was used as a scavenger, for both substrates. The resolution of the fabricated microstructure depended strongly on the composition of the electrolyte, and especially on the concentration ratio of l-cystine to Br^-. A well-defined, polished Pt microcylindrical electrode was employed to examine the deviation of the size of the etched spots from the real diameter of the microelectrode. The thickness of the confined etchant layer can be estimated, and thus the composition of the electrolyte can be optimized for better etching precision. The etched patterns were approximately negative copies of the mold, and the precision of duplication could reach the micrometer level for p-Si and the submicrometer level for n-GaAs. Although the same etchant (Br_2) and scavenger (l-cystine) were used in the etching solutions for GaAs and Si, the etching process, or mechanism, is completely different in the two cases. Compared with the fast etching process on GaAs in an etching solution with a concentration ratio of 3:1 of l-cystine to Br^-, the concentration ratio needs to be 50:1 for etching of Si. For the micromachining of Si, the addition of a cationic surfactant (cetyltrimethylammonium chloride, CTACl) is necessary to reduce the surface tension of the substrate and hence reduce the influence of evolution of the byproduct H_2. The function of the surfactant CTACl in comparison with an anionic surfactant (sodium dodecyl sulfate) was studied in contact-angle experiments and micromachining experiments and then is discussed in detail.

1. Introduction

Silicon is the most important material for micro-electromechanical systems (MEMS) owing to its excellent electronic and mechanical properties.[1,2] Gallium arsenide (GaAs) is another important compound semiconductor, which is widely used in high-speed and high-temperature components, optoelectronic devices, and force and resonant sensors.[3−6] The micromachining of these two materials down to micrometer or even submicrometer dimensions is considered to be a key technology in MEMS. Previously, a lithographic method has been used successfully for the fabrication of two-dimensional (2D) micromechanical devices in batch processes.[7,8] However, to extend and strengthen the working functions of MEMS for more applications, more complex microstructures or truly three-dimensional (3D) structures need to be fabricated. Therefore, advanced micromachining technologies need to be developed further.

Recently, many novel approaches have been proposed for 3D microfabrication on semiconductors. The electrochemical micromachining method is considered to be hopeful; this includes several new methods, such as electro-micromachining using ultrashort pulses, proposed by Schuster et al.,[9−11] a localized etching method using a SECM (scanning electrochemical microscope), proposed by Fan and Bard,[12−15] electrochemical etching on a lithographically prestructured n-Si surface, developed by Lehmann and by Kleimann et al.,[16−21] and electrochemical scanning probe lithography (SPL) methods.[11,22−25] Although these methods have a good potential for application, the fabrication of 3D structures in a batch has been only partially realized. For example, localized etching or deposition can be accomplished down to micrometer or even nanometer scales using a SECM or SPL, but these techniques work mainly in a "point by point" direct way, and hence it is very time-consuming to fabricate a complicated 3D microstructure. Electrochemical micromachining using nanosecond pulses has been successfully used to fabricate various 3D structures on metal surfaces,[10,26,27] but only simple microstructures, including holes and channels, can be formed on high-doped p-Si. The applied pulses have to be shorter than ∼3 ns to fabricate microstructures with a precision of 1 μm on low-doped p-Si owing to the high resistance of the substrate and the large extent of the space charge layer. [9] Kleimann et al. have fabricated high-aspect-ratio needles, tubes, and walls down to the nanometer range by using electrochemical etching on n-Si, but complex 3D structures such as hemispheres and cones are not achievable.[20,21]

Tian et al. have proposed an alternative effective method for 3D micromachining, called the confined etchant layer technique (CELT) (Figure 1). This technique can fabricate 3D micro-

* E-mail: jingtang@xmu.edu.cn, caoguohui@hit.edu.cn
[†] Xiamen University.
[‡] Harbin Institute of Technology.

10.1021/jp063110m CCC: $33.50
Published on Web 08/30/2006

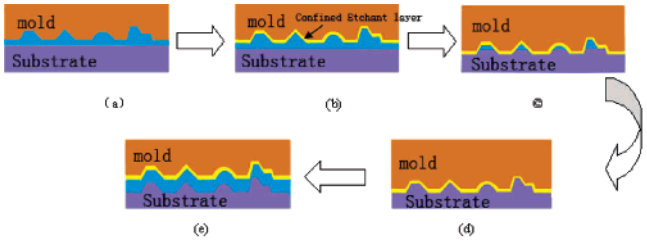

Figure 1. Schematic illustration of principle of confined etchant layer technique (CELT).

structures on different kinds of substrate in a batch, and its mechanism is illustrated in the references.[28−32] When the potential of the mold with a 3D pattern (the working electrode) is controlled appropriately, the etchant species is electrochemically generated at the mold surface and diffuses into the bulk electrolyte. The thickness of the diffusion layer is generally several tens of micrometers. However, after adding a "scavenger" into the electrolyte that can react quickly with the etchant (e.g. within microseconds, on average), the concentration gradient of the etchant can be greatly enhanced. The thickness of the confined etchant layer (CEL) can be greatly decreased to several tens of nanometers as shown in Figure 1b. In the beginning of micromachining, partially etched microstructures are obtained on the workpiece (Figure 1c). When the mold is controlled precisely to approach forward, a whole negative pattern of the mold can be transferred into the workpiece (Figure 1d). As a result, the 3D pattern of the mold can be replicated on the etched substrate. This Figure demonstrates the key feature of the CELT to be distance sensitive, and this characteristic allows the arbitrary 3D microstructures to be replicated on the substrate in a simple, maskless process regardless of the surface roughness of the workpiece.

Here, we present the use of CELT to fabricate complex 3D microstructures on n-GaAs and p-Si. The optimal composition of the etching solutions for fabricating 3D patterns on p-Si and n-GaAs with micrometer or submicrometer resolution has been studied. The differences in the mechanism of the etching process between the micromachining of p-Si and n-GaAs will be discussed.

2. Experimental Details

The experimental setup has been described elsewhere.[28−32] The workpiece was fixed at the bottom of a Teflon cell in the micromachining experiments. An instrument composed of a stepping motor and a piezoelectric tube under computer control could monitor the movement of the mold electrode relative to the substrate, with a step size from 50 nm to 50 μm.

The workpieces to be etched were n-GaAs(100) and p-Si-(100) wafers (Huajing Electronic Corporation, Wuxi, China). The 300 μm thick GaAs wafer was doped with Si, and the carrier concentration n ranged from 1.0×10^{18} to 4.31×10^{18} cm^{-3}. The 525-μm thick Si wafer was boron-doped, with a resistivity of 0−20 Ω cm. Before mounting in the electrochemical cell, the Si wafer was cleaned with H_2SO_4 and H_2O_2 (4:1), the native oxide layer was removed by dipping in 10% HF solution, and the wafer was then rinsed with ultrapure water. The preparation of the GaAs workpiece was done by simply rinsing with acetone and water.

The mold generating the etchant was used as the working electrode in a three-electrode system. A Pt wire ring surrounding the working electrode and a saturated calomel electrode (SCE) were used as the counter electrode and the reference electrode, respectively. The workpiece was left at open-circuit in the solution. Three kinds of mold were used in the etching experiments. One was a microcylindrical electrode made of Pt wires (Alfa, 99.99%) with a diameter of 250 μm or 50 μm. The wires were coated completely with epoxy resin and then polished with sandpaper until the wire was exposed. They were polished further with a series of alumina powders with diameters of 2, 1, and 0.05 μm successively. Finally, acetone was used to dissolve the epoxy resin on the top end of the wire, which was then rinsed in water in an ultrasonic bath. The second kind of mold was a titanium plate with a hexagonal array of hemispherical cavities (diameter 104.7 μm). This was fabricated by a through-mask electrochemical micromachining technique developed by Landolt's group. [33] The titanium plate was attached to the holder in the CELT instrument by conductive silver glue. To make a Pt-covered surface, a 200 nm thick Pt film was deposited on the mold surface by radio frequency magnetron sputtering. The third kind of mold was fabricated by an electric-discharge machining (EDM) technique. This Pt−Ir (80% Pt) mold included 3D microstructures made up of grooves tens of micrometers wide, forming the logo "XMU" of Xiamen University, and three hemispherical cavities with diameters of hundreds of micrometers.

All the micromachining experiments were done by controlling the mold so that it was at a fixed distance of a few hundreds of nanometers above the substrate surface. The working procedure was as follows. The mold was brought slowly down until a sudden rise in the force between the mold and the substrate was detected. To protect the mold from crashing, the value of the force must be below 1 mN. The mold was then withdrawn to a fixed position away from the substrate by means of the piezoelectric tube. When the initial distance between the substrate and the mold is small enough and less than the thickness of the CEL, a 3D microstructure can be fabricated on the surface of the workpiece using the CELT mechanism.

All of the electrochemical measurements were made with a CHI 631B electrochemical workstation. The electrochemical measurements were performed using a Pt polycrystalline electrode in a Teflon cell. The microstructures of the mold and the etched workpieces were characterized with a confocal microscope (Olympus 2000) and an optical microscope (Leica Q550MW). Contact-angle measurement was done with a measuring system made by ourselves.

3. Results and Discussion

3.1. Study of Composition of Etching Solution. *3.1.1 Solution for p-Si Micromachining.* The selection of an effective etchant and a suitable scavenger is one of the key issues that must be resolved to utilize CELT in micromachining. Mandler and Meltzer[15] have indicated that Si can be locally etched in hydrofluoric acid by electrogenerating Br_2 at a Pt electrode that was held close to a Si wafer. Similarly, electrogenerated Br_2 was also used as an etchant in our study. In our previous work,[30,32] H_3AsO_3 was found to be a good scavenger to react quickly with Br_2, but H_3AsO_3 has a poisonous nature and an acute toxicity so that the solution containing H_3AsO_3 is associated with the environmental pollution problem that limits its application in industry. Instead, in view of the fast reaction between l-cystine and Br_2 used to synthesize l-cysteic acid by organic electrochemistry,[34,35] we chose l-cystine (RSSR, R = $CH_2CH(NH_2)COOH$) as a new scavenger to replace AsO_3^{3-} in our experiments on 3D micromachining of n-GaAs and p-Si.

Figure 2 shows cyclic voltammograms of a polycrystalline Pt electrode obtained using solutions with various concentrations of l-cystine and HBr. In all curves, the concentrations of H_2SO_4,

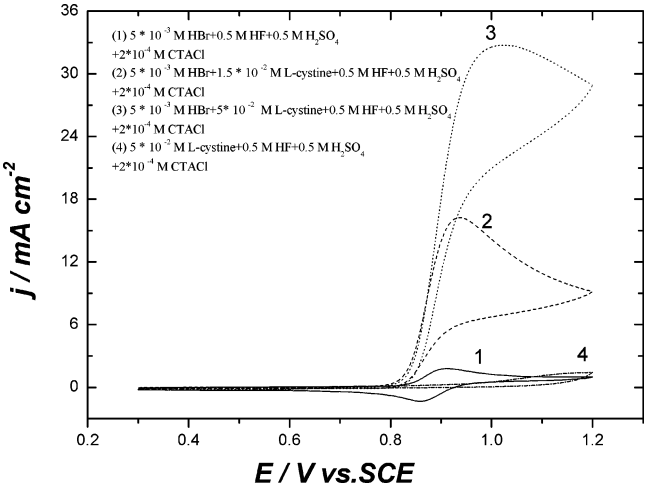

Figure 2. Cyclic voltammograms of a Pt polycrystalline electrode in the etching system for p-Si in the presence of different concentrations of l-cystine and KBr: (1) 5×10^{-3} M HBr + 0.5 M HF + 0.5 M H_2SO_4 + 2×10^{-4} M CTACl; (2) 5×10^{-3} M HBr + 0.5 M HF + 0.5 M H_2SO_4 + 2×10^{-4} M CTACl + 1.5×10^{-2} M l-cystine; (3) 5×10^{-3} M HBr + 0.5 M HF + 0.5 M H_2SO_4 + 2×10^{-4} M CTACl + 5×10^{-2} M l-cystine; (4) 0.5 M HF + 0.5 M H_2SO_4 + 2×10^{-4} M CTACl + 5×10^{-2} M l-cystine. Scan rate: 50 mV/s.

HF, and CTACl (cetyltrimethylammonium chloride) were fixed. CTACl is a surfactant, whose function in the micromachining will be discussed in detail in Section 3.2. Curve 1 in Figure 2 was observed to show a peak current density of approximately 1.8 mA/cm^2 in a solution without l-cystine. The pair of peaks appearing at 0.9 V corresponds to the reversible oxidation of Br^-. Curves 2 and 3 show that the current density of Br^- oxidation increases gradually with increasing concentration of added l-cystine When the concentration ratio of l-cystine to Br^- is 3:1 (curve 2) and 10:1 (curve 3), the current density corresponding predominantly to Br^- oxidation increases to 16.3 mA/cm^2 and 32.6 mA/cm^2, respectively. Fortunately, the electrooxidation behavior of l-cystine at 1.0 V, shown in curve 4, gives a comparatively small current density of 0.5 mA/cm^2, and this process did not influence the chemical reaction between Br_2 and l-cystine. Obviously, the cyclic voltammograms show that the electrochemical behavior of the Pt electrode in an etching solution containing HBr and l-cystine obeys the rule of a homogeneous electrocatalytic reaction. Here we call the homogeneous chemical reaction the "scavenging reaction". The significant increase in the oxidation current density illustrates that Br_2 can be quickly consumed by l-cystine and Br^- can be regenerated homogeneously near the Pt electrode surface. Therefore, it can be concluded that l-cystine has a high capability as a scavenger for Br_2.

This cyclic voltammetric experiment indicates qualitatively that l-cystine is an appropriate scavenger for Br2. According to the principle of CELT, the etching resolution is determined by the thickness of the CEL (μ); we can deduce theoretically that it depends on the diffusion coefficient of the etchant (D) and on the pseudo-first-order reaction rate of the scavenger with Br_2 (Ks):[31]

$$\mu = (D/Ks)^{1/2} \quad (1)$$

The theoretical thickness of the CEL in the etching solution is calculated to be around 41 nm, since the reaction rate constant Ks is 7×10^5 s^{-1} (high) and the value of D is 1.2×10^{-5} cm^2 s^{-1}. [36] However, the conditions in the etching experiment are more complicated than in the theoretical hypothesis. Therefore,

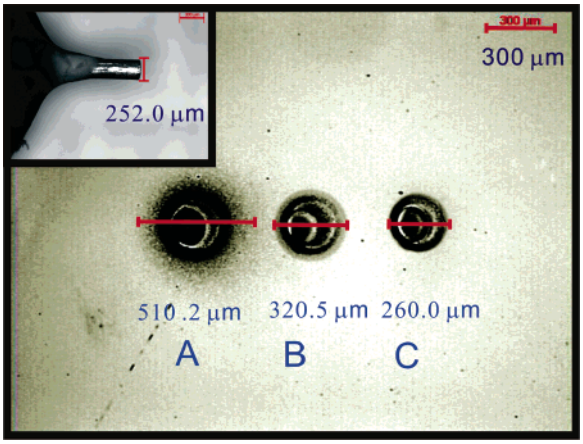

Figure 3. Microscope image of Si microstructure etched in solutions of (A) 5×10^{-3} M HBr + 0.5 M HF + 0.5 M H_2SO_4 + 2×10^{-4} M CTACl; (B) 5×10^{-3} M HBr + 0.5 M HF + 0.5 M H_2SO_4 + 2×10^{-4} M CTACl +1.5×10^{-2} M l-cystine; (C) 5×10^{-3} M HBr + 0.5 M HF + 0.5 M H_2SO_4 + 2×10^{-4} M CTACl + 5×10^{-2} M l-cystine. The potential of the Pt electrode was 1.0 V vs SCE, and the etching time was 10 min. The distance between the Pt microelectrode and the Si was 250 nm. The insert is a microscope image of the Pt microcylindrical electrode (diameter = 252.0 μm)

it is very necessary to find a more convenient and straightforward way to evaluate the resolution of CELT in a quantitative or semiquantitative way. Here, we used a Pt microcylindrical electrode as a mold, and the etching resolution was estimated by inspecting the deviation of the sizes of the etched spots from the real mold diameter. Figure 3 shows a well-polished Pt microcylindrical electrode with a diameter of 252.0 μm, and the patterns etched on the p-Si material when the distance between the mold and the p-Si was less than the thickness of the CEL. Three different etching solutions were applied in the electrochemical micromachining experiments. During the whole etching process, the potential applied to the microelectrode was kept at 1.0 V vs SCE for 10 min. The mechanism of the etching process can be expressed as follows:

Generation reaction at tip:

$$10Br^- \rightarrow 5Br_2 + 10e \quad (2)$$

Homogeneous scavenging reaction:

$$5Br_2 + RSSR + 6H_2O \rightarrow 2RSO_3H + 10H^+ + 10Br^- \quad (R = CH_2CH(NH_2)COOH) \quad (3)$$

Heterogeneous surface etching reaction:

$$Br_2 + Si + 6HF + 4e_{CB}^- \rightarrow 2\,Br^- + SiF_6^{2-} + 3H_2 \quad (4)$$

In the case of spot A in Figure 3, the diameter is the largest of all the etched spots because the Br_2 electrogenerated on the mold has diffused quickly into the solution without the homogeneous scavenging reaction. Hence the etched pattern will be much larger than the real tip diameter. Assuming that the etching precision is $P = (\Phi_{etched} - \Phi_{electrode})/2$ and the machining error is $E = P/\Phi_{electrode} \times 100\%$, where Φ_{etched} and $\Phi_{electrode}$ are the diameters of the etched pattern and the microelectrode, respectively, P for spot A is (510.2−252.0)/2 = 129.1 μm, and E is 129.1/252.0 × 100% = 51.2%. In the case of spot B, the micromachining was done in a solution with a 3:1 concentration ratio between l-cystine and HBr, and here P is 34.3 μm and E is 13.5%. When the concentration ratio is 10:1, in a solution of 5×10^{-3} M HBr + 5×10^{-2} M l-cystine + 2×10^{-4} M CTACl + 0.5 M H_2SO_4 + 0.5 M HF, the diameter of the etched spot C (260.0 μm) matches that of the

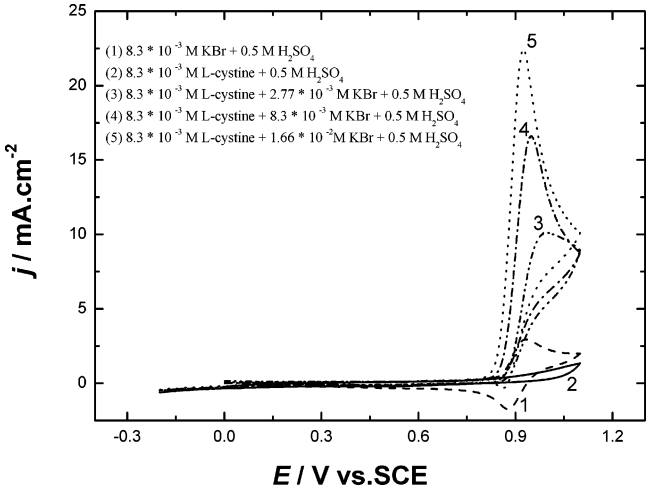

Figure 4. Cyclic voltammograms of a Pt polycrystalline electrode in the etching system for n-GaAs in the presence of different concentrations of l-cystine and KBr: (1) 8.3×10^{-3} M KBr + 0.5 M H_2SO_4; (2) 8.3×10^{-3} M l-cystine + 0.5 M H_2SO_4; (3) 8.3×10^{-3} M l-cystine + 2.77×10^{-3} M KBr + 0.5 M H_2SO_4; (4) 8.3×10^{-3} M l-cystine + 8.3×10^{-3} M KBr + 0.5 M H_2SO_4; (5) 8.3×10^{-3} M l-cystine + 1.66×10^{-2} M KBr + 0.5 M H_2SO_4. Scan rate: 50 mV/s.

Pt microcylindrical electrode much more precisely, and the machining error is only 1.6%. The best etching precision for p-Si in the experiments is 1.0 μm, and it is very difficult to achieve submicrometer precision, owing to the mechanism of etching in HF, which will be discussed in comparison with the following experiments on micromachining of GaAs.

3.1.2. Solution for n-GaAs Micromachining. Since Br_2 can etch GaAs homogeneously,[12,13] the same etchant and scavenger were used for the micromachining of GaAs. Here we optimized the solution composition for n-GaAs etching in the same way as for p-Si. Figure 4 shows the electrochemical behavior of a Pt electrode in solutions with different composition ratios of KBr and l-cystine. The concentration of KBr was varied here, instead of that of l-cystine as in the case of p-Si. This figure demonstrates the same tendency as in Figure 2: the anodic current density corresponding to Br^- oxidation increases with an increase in the concentration ratio of l-cystine to KBr. For example, curves 4 and 1 are cyclic voltammograms for solutions with and without l-cystine, respectively. The current density in curve 4 shows a 7-fold increase over that in curve 1, at 0.9 V. While the concentration of Br^- in curve 3 decreases to one-third of that in curve 1, the oxidation current density of Br^- increases to 3 times that in curve 1. This indicates that Br_2 electrogenerated on the electrode is quickly destroyed by l-cystine, which leads to a very high concentration of Br^- near the electrode.

Figure 5 shows the etched patterns obtained by using a Pt microcylindrical electrode (50.0 μm) as the mold. The concentration of KBr was varied here. However, a decrease in the thickness of the CEL with an increase in the concentration ratio between l-cystine and Br^- is again observed. The mechanism of the GaAs etching process can be expressed as follows:

$$\text{Surface etching reaction:} \quad 6Br_2 + 2GaAs + 6H_2O \rightarrow 2Ga^{3+} + 2AsO_3^{3-} + 12Br^- + 12H^+ \quad (5)$$

In the case of spot A, without scavenger, shown in Figure 5, the etching precision P is $(65.7-50.0)/2 = 7.85$ μm, and the machining error E is $7.85/50 \times 100\% = 15.7\%$. The concentration of KBr decreases from spot B to spot D, and the ratio of l-cystine to Br^- increases from 1:2 to 3:1. The sizes of the etched

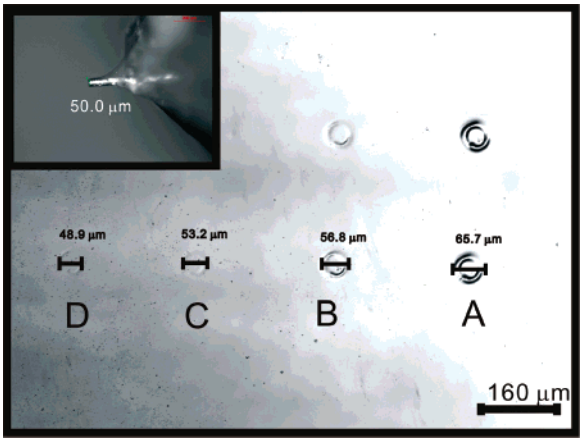

Figure 5. Microscope images of GaAs microstructure etched in solutions of (A) 8.3×10^{-3} M KBr + 0.5 M H_2SO_4; (B) 8.3×10^{-3} M l-cystine $+1.66 \times 10^{-2}$ M KBr + 0.5 M H_2SO_4; (C) 8.3×10^{-3} M l-cystine + 8.3×10^{-3} M KBr + 0.5 M H_2SO_4; (D) 8.3×10^{-3} M l-cystine + 2.77×10^{-3} M KBr + 0.5 M H_2SO_4. The potential of the Pt electrode was 1.0 V vs SCE, and the etching time was 20 min. The distance between the Pt microelectrode and the GaAs was 250 nm. The insert is a microscope image of the Pt electrode (diameter = 50 μm).

TABLE 1: Etching Precision and Machining Error of Micromachining on p-Si and n-GaAs using Pt Microcylindrical Electrode as a Mold

concentration ratio of l-cystine to Br^-		no scavenger	1:1	3:1	10:1	50:1
etching precision (μm)	Si	129.1		34. 3	4.0	1.0
	GaAs	7.85	1.6	0.55		
machining error (%)	Si	51.2		13.5	1.6	0.4
	GaAs	15.7	3.2	1.1		

spots decrease and reach the diameter of the microelectrode. Submicrometer precision was obtained with spot D, with an etching precision of about 0.55 μm and a machining error of about 1.1%.

In summary, the etching precision can be evaluated in a semiquantitative way from etching experiments using a Pt microcylindrical electrode rather than by complicated theoretical simulation. These results also make information available about microfabrication with complex 3D molds.

3.1.3. Comparison between the Etching Solutions for n-GaAs and p-Si. The experiments described above indicate that l-cystine is an effective scavenger for electrogenerated Br_2. Micrometer and submicrometer precision can be achieved in appropriate etching systems. It is interesting to note that the etching precisions for GaAs and Si are different despite having the same concentration ratio of l-cystine to Br^-. For instance, spot A in Figure 3 and spot A in Figure 5 were both fabricated using a solution without l-cystine, but the machining errors are 51.2% and 15.7%, respectively. The etching precision is 0.55 μm for spot D in Figure 5, but that for spot B in Figure 3 is 34.3 μm, and both spots were etched in a solution with the same concentration ratio of l-cystine to Br^- (3:1). Table 1 shows the etching precision and machining error of microfabrication on p-Si and n-GaAs in various solutions, obtained by using a Pt microcylindrical electrode as a mold.

On the basis of the mechanism of CELT illustrated in eq 1, the etching precision depends on the rate of the homogeneous scavenging reaction and the diffusion coefficient of the etchant Br_2. But our results show that the heterogeneous reaction between the etchant and the substrate dramatically affects the etching precision, and this phenomenon has been well studied

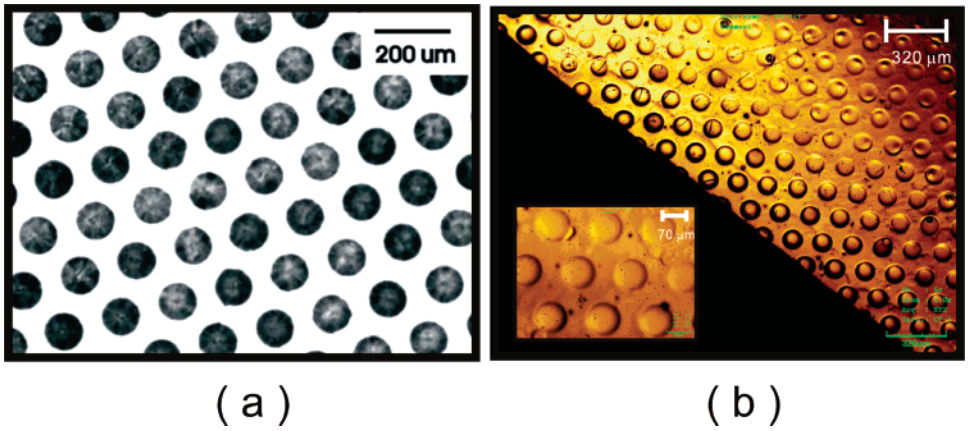

Figure 6. (a) Microscope image of the mold containing a microhemispherical cavity array, and (b) the GaAs microstructure, etched in a solution of 8.3×10^{-3} M l-cystine + 2.77×10^{-3} M KBr + 0.5 M H_2SO_4. The potential of the mold was 1.0 V vs SCE, and the etching time was 20 min. The distance between the mold and the GaAs was 250 nm. The insert is a microspcope image with a better magnification.

by SECM in Bard's papers.[14] In Bard's study, the etching of copper using electrogenerated $Os(bpy)_3^{3+}$ can reach high resolution or precision because of a fast heterogeneous surface etching reaction directly beneath the electrode. The $Os(bpy)_3^{3+}$ electrogenerated at the electrode can be consumed quickly by reaction with the Cu substrate so that lateral diffusion of the etchant is almost absent.

It can be concluded from our etching experiments in the solutions without scavenger that the etching speed for Br_2 on n-GaAs is much faster than on p-Si. This is because the etching of these two semiconductors proceeds by different mechanisms. The etching of n-GaAs is a very fast process with a direct chemical decomposition, as shown in eq 5.[13,15,37] In the etching of Si, the initial step is a chemical process of attack on a Si−Si back-bond and formation of silicon hydride products as surface state intermediates.[15,38] The rate-limiting step is where the intermediates react with HF to give rise to hydrogen evolution and SiF_6^{2-}, as shown in eq 4. This difference in mechanism explains why the micromachining of GaAs can easily attain high resolution, unlike Si micromachining. When Si etching proceeds in a solution without scavenger or with a low concentration of l-cystine, the Br_2 is only partially depleted, owing to the slow reaction rate, and the remaining etchant easily diffuses in the lateral direction, resulting in a much larger etching pattern. As the concentration of scavenger increases, the etchant diffusion layer is confined to the vicinity of the electrode surface and the etching precision gradually improves. Compared with the fast etching process on GaAs, the concentration ratio of the scavenger to HBr needs to be larger (50:1) than the value of 3:1 (l-cystine: KBr) used with GaAs to reach micrometer resolution.

Furthermore, it is very necessary to mention the depth of the microfabricated holes is not equal to the thickness of CEL as shown in Figure 3 and Figure 5. Actually, the depth of fabricated microstructure by CELT is closely related with several factors, including the total amount of the etchant in the very thin CEL, the distance between the substrate and the mold, and the reaction rate between the etchant and the substrate. The tendency of the decrease of the depth of microfabricated holes with the increase of the scavenger concentration is observed in Figure 3. The AFM characterization also revealed the depths of the well-replicated microholes by CELT are mostly under one micrometer without approaching of the mold to the GaAs or Si. To fabricate deeper microstructures, it is mandatory to renew the electrolyte beneath the mold from the bulk solution owing to the depletion of the scavenger in the center of the mold. The present solution is by approaching and then lifting the mold for several times in order to renew the scavenger underneath the electrode. A 6 μm deep hole has been fabricated on the n-GaAs by such a time-consuming process. Since this process is also easily influenced by a lot of unpredictable factors, a larger etching precision is achieved after feeding the mold for several times.

3.2. Micromachining with 3D Complex Molds. *3.2.1. Micromachining of n-GaAs with a Mold Containing an Array of Hemispherical Cavities.* In previous studies,[30] Sun et al. etched n-GaAs using a gear-like microstructure fabricated by a bulk-Si etching technique. In our study, a Pt mold with a hexagonal array of hemispherical cavities was employed. Following the results of the micromachining experiments using a Pt microcylindrical electrode, the concentration ratio of l-cystine to Br^- used was 3:1, and the composition of the etching solution was 0.5 M H_2SO_4 , 8.3×10^{-3} M l-cystine, and 2.77×10^{-3} M KBr. The distance between the mold and the GaAs was kept constant at ca. 250 nm.

Figure 6 shows optical images of this complex mold and the etched pattern on n-GaAs. The diameter of the hemispherical cavities was 104.7 μm. A hexagonal pattern of convex features with an average diameter of 103.0 μm was fabricated on the surface of the n-GaAs, and the resolution of the micromachining was measured to be in the region of hundreds of nanometers.

Because the parallelism between the GaAs surface and the Pt mold was adjusted only by eye and gradienter, the initial distance between each cavity in the mold and the substrate varied over the area of the mold, and hence the height of the fabricated array was not uniform over the n-GaAs. The results indicate that CELT is a distance-sensitive technique. Here, we also observe the differences in shape and depth between the mold and the microfabricated structure, since the mold did not approach the substrate stepwisely as shown in the Figure 1. The fabricated microstructures are convex features with a height of less than 1 μm measured from AFM (atomic force microscope), but the cavities in the mold are hemispheres with a depth of tens of micrometers. To achieve a completely negative copy of the mold, it would be essential for the mold to approach the substrate stepwisely till the whole microstructures on the mold was replicated on the workpiece. A study of this is still under way in our laboratory.

3.2.2. Micromachining on p-Si with a 3D Pt−Ir Mold. The above mold with an array of hemispherical cavities was not available for a study of micromachining of Si, since the Ti substrate had a low ability to resist corrosion by HF, especially during the etching of Si. Instead, a 3D mold was fabricated

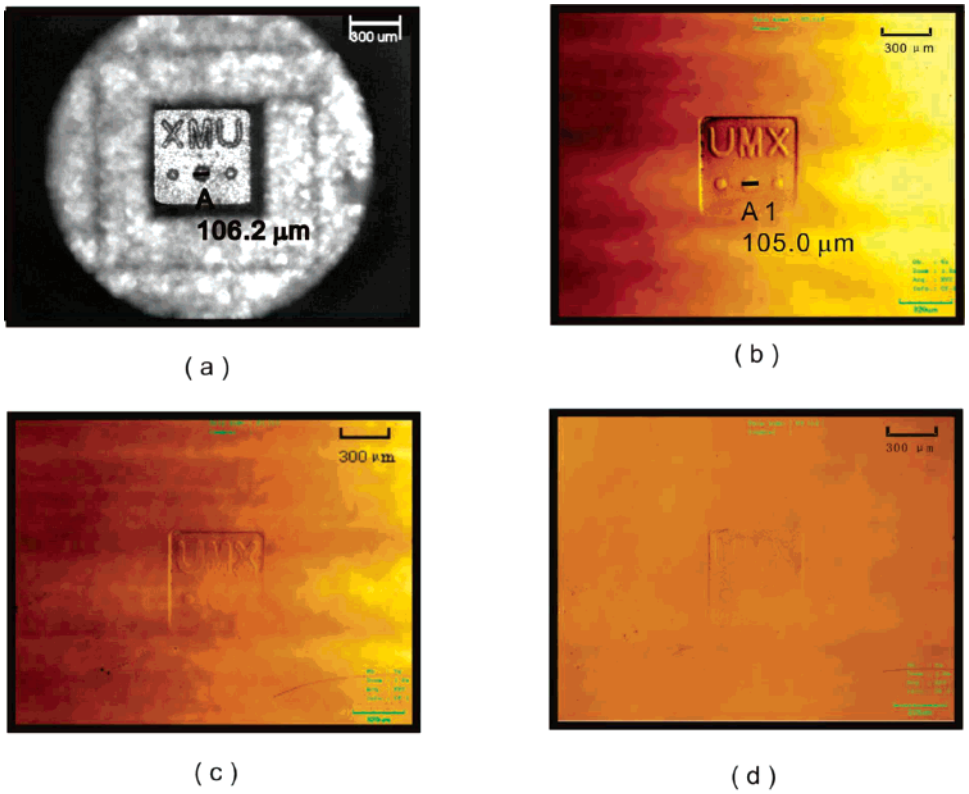

Figure 7. (a) Microscope image of 3D Pt−Ir mold; (b) Si microstructure etched in a solution of 1×10^{-3} M HBr + 5×10^{-2} M l-cystine + 2×10^{-4} M CTACl + 0.5 M H_2SO_4 + 0.5 M HF; (c) Si microstructure etched in a solution of 1×10^{-3} M HBr + 5×10^{-2} M l-cystine + 0.5 M H_2SO_4 + 0.5 M HF; (d) Si microstructure etched in a solution of 1×10^{-3} M HBr + 5×10^{-2} M l-cystine + 2×10^{-4} M SDS + 0.5 M H_2SO_4 + 0.5 M HF. The potential of the mold was 1.0 V vs SCE, and the etching time was 10 min. The distance between the mold and the Si was 250 nm.

from bulk Pt−Ir by EDM, as shown in Figure 7a, and this kind of mold is very stable in an etching solution containing HF.

On the basis of the micromachining experiments with a Pt cylindrical electrode described in Section 3.1.1, the concentration ratio of l-cystine to HBr was chosen to be greater than 50:1. To achieve 1 mm resolution, the etching experiment was performed in 1×10^{-3} M HBr + 5×10^{-2} M l-cystine + 2×10^{-4} M CTACl + 0.5 M H_2SO_4 + 0.5 M HF. During the etching process, the potential applied to the mold was kept at 1.0 V versus SCE, and the distance between the mold and the Si was kept constant at about 250 nm. The confocal microscope image shown in Figure 7b shows that the etched structure is a fine, negative etched copy of the mold. The sizes of the protruding ridge and the three hemispherical convex features were approximately those of a negative copy of the mold. The resolution of the micromachining is deduced to be around 1 μm from the difference between the diameter of the convex feature marked A1 (diameter = 105.0 μm) in Figure 7b and that of the concave feature marked A (diameter = 106.2 μm) in Figure 7a.

In the process of micromachining on p-Si, hydrogen is evolved owing to the chemical mechanism illustrated in eq 4. Figure 7c shows the etched pattern achieved in a solution without CTACl, and there is only a blurred etched profile on the p-Si. The hydrogen is trapped on the highly hydrophobic Si surface, in the etching solution, rather than escaping from the narrow gap (250 nm) between the mold and the Si during the process of micromachining in HF. Therefore, the increasing concentration of hydrogen during the etching process influences the subsequent etching process, since the hydrogen bubbles mask the mold surface from the electrolyte. A similar phenomenon has been observed in the electrochemical preparation of porous Si in hydrofluoric acid, where hydrogen bubbles stick to the Si surface and result in an inhomogeneous porous layer.[39] If organic species such as ethanol or surfactants are added, the wettability of porous Si is enhanced and the surface tension at the Si-solution interface is dramatically reduced. Hence the bubbles can escape easily and a more uniform porous layer is achievable.[19,39−42] Similarly, we added a low concentration of a surfactant, such as the cationic surfactant CTACl, to reduce the surface tension, and in this case the influence of hydrogen evolution can be almost neglected.

TABLE 2: Contact Angles of Three Solutions on the Si Surface Investigated

solution	no surfactant	SDS added	CTACl added
contact angle (deg)	80	24	37

In addition, the anionic surfactant SDS (sodium dodecyl sulfate) was also studied to understand the function of the surfactant during the micromachining process.[42] Figure 7d shows a confocal-microscope image of the etched pattern obtained in a solution containing SDS. It is amazing that the etching resolution is even worse than that without surfactant, and there is no clear negative copy of the mold. Table 2 gives the contact angles of the three kinds of electrolyte on the p-Si surface after pretreatment in HF. The contact angles of the solutions containing SDS and CTACl are 24° and 37°, respectively. This indicates that either anionic or cationic surfactants can reduce the surface tension and enhance the wettability of the Si surface. Theoretically, the hydrogen bubbles are expected to escape from the Si surface when either of these two surfactants is added, and then microstructures should be obtained with high resolution. However, the experimental results are in contradiction with

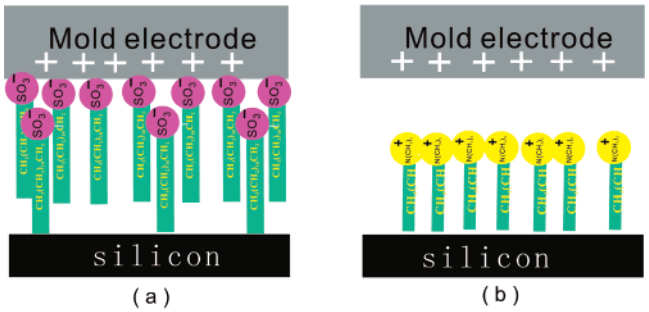

Figure 8. The mechanism by which the influence of H_2 bubbles is decreased by adding the surfactants (a) SDS and (b) CTACl.

the contact angle measurements, since the etching resolution decreased dramatically after addition of SDS.

We have proposed a model to explain in detail how the surfactant influences the micromachining process. This model considers the different chemical structures of surfactants and the change in the polarity, which may lead to a different behavior in the presence of an electric field around the mold during the etching process. The anion or cation of the surfactant is drawn in Figure 8 as a tadpole-like structure with a charged hydrophilic head and a long hydrophobic tail composed of carbon chains. During the whole etching process, the potential applied to the mold was kept at 1.0 V versus SCE, and the mold was thus positively charged when it was held very close to the Si surface. Therefore, the anionic surfactant SDS can adsorb strongly at the positively charged mold surface, as shown in Figure 8a, owing to the electrostatic force between the negatively charged head of the surfactant and the mold. Since most of the SDS molecules adsorb on the mold surface by the negatively charged head, as shown in Figure 8a, they cannot reduce the surface tension at the Si−solution interface. Simultaneously, the Br^- oxidation at the mold surface is markedly decreased, since the strong adsorption of SDS prevents the diffusion of Br^- from the solution to the electrode, leading to less Br^- oxidation on the mold. As shown in Figure 8b, however, the hydrophobic tail of CTACl can be strongly adsorbed on the Si surface, since the Si was pretreated in HF to form hydrophobic Si−H bonds on the surface.

The influence of the surfactant can be also obviously observed in the chronoamperometry $I-t$ curve recorded during the micromachining process. Figure 9 gives a curve of the oxidative current of Br^- on the Pt−Ir mold electrode versus time, measured at a constant potential of 1.0 V during the etching process. Curves 1−3 correspond to the results obtained in solutions without surfactant, with SDS, and with CTACl, respectively. It is apparent that the current density for curve 3 is about three times higher than for curves 1 and 2. On the basis of the above discussion, we can conclude that the CTACl surfactant can efficiently remove hydrogen bubbles trapped on the Si surface, and the current density hence increases greatly, without the influence of bubbles. In contrast, the current density in curve 2, for SDS, decreases dramatically and is even lower than that in curve 1, without surfactant. This is further proof that SDS mostly adsorbs on the Pt−Ir mold instead of on the interface of the Si and simultaneously disturbs the diffusion of Br^- to the mold surface to be oxidized.

4. Conclusion

We have demonstrated that 3-D micromachining by indirect electrochemical etching of n-GaAs and p-Si can be accomplished using CELT with appropriate etching solutions. The success of this process depends mainly on the concentration

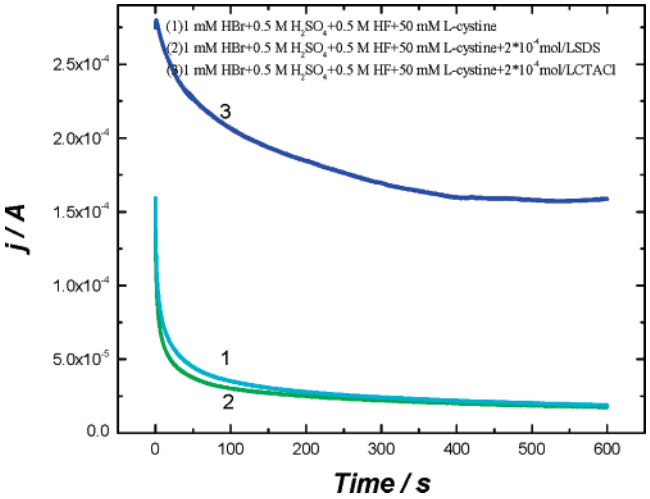

Figure 9. Curves of the oxidative current of the Pt−Ir mold vs time, measured during the microfabrication process on p-Si in solutions of (1) 1×10^{-3} M HBr + 5×10^{-2} M l-cystine + 0.5 M H_2SO_4 + 0.5 M HF; (2) 1×10^{-3} M HBr + 5×10^{-2} M l-cystine + 2×10^{-4} M SDS + 0.5 M H_2SO_4 + 0.5 M HF; (3) 1×10^{-3} M HBr + 5×10^{-2} M l-cystine + 2×10^{-4} M CTACl + 0.5 M H_2SO_4 + 0.5 M HF. The potential of the Pt electrode was 1.0 V vs SCE, and the etching time was 10 min. The distance between the mold and the Si was 250 nm.

ratio of l-cystine to Br^- in the etching solution. The micromachining experiments show that l-cystine is an effective scavenger for electrogenerated bromine, and that submicrometer precision can be achieved in appropriate etching systems. The etched patterns on GaAs and Si match approximately the mold size and retain the complex mold shape. The difference between the etching systems for n-GaAs and p-Si indicates that the etching precision also depends strongly on the heterogeneous reaction between the electrogenerated species and the substrate, as well as on the scavenging process. In the case of micromachining on Si, the byproduct hydrogen greatly affects the etching resolution, and high-resolution etched patterns can be achieved on p-Si only after adding the cationic surfactant CTACl.

Acknowledgment. Support for this research by the National Science Foundation of China (20503024) and by funds from Fu Jian Province (E0520001) is gratefully acknowledged. The titanium mold with an array of hexagonally arranged hemispherical cavities was kindly provided by Professor Dieter Landolt of the Swiss Federal Institute of Technology, Lausanne. The Pt−Ir mold prepared by the EDM technique was provided by Dr. Guo H. Cao of the Harbin Institute of Technology, China. The authors acknowledge Prof. Zhong Q. Tian of the Xiamen University for helpful discussions.

References and Notes

(1) Gardner, J. W.; Varadan, V. K.; Awadelkarim, O. O. In *Microsensors, MEMS, and Smart Devices*; John Wiley & Sons: Chichester, U.K., 2001.

(2) Petersen, K. E. *Proc. IEEE* **1982**, *70*, 420.

(3) Dehe, A.; Fricke, K.; Hartnagel, H. L. *Sens. Actuators, A* **1995**, *47*, 432.

(4) Fricke, K. *J. Appl. Phys.* **1991**, *70*, 914.

(5) Hjort, K.; Soderkvist, J.; Schweitz, J. A. *J. Micromech. Microeng.* **1994**, *4*, 1.

(6) Ribas, R. P.; Leclercq, J. L.; Karam, J. M.; Courtois, B.; Viktorovitch, P. *Mater. Sci. Eng., B* **1998**, *51*, 267.

(7) Kovacs, G. T. A.; Maluf, N. I.; Petersen, K. E. *Proc. IEEE* **1998**, *86*, 1536.

(8) Lang, W. *Mater. Sci. Eng., R* **1996**, *17*, 1.

(9) Allongue, P.; Jiang, P.; Kirchner, V.; Trimmer, A. L.; Schuster, R. *J. Phys. Chem. B* **2004**, *108*, 14434.

(10) Schuster, R.; Kirchner, V.; Allongue, P.; Ertl, G. *Science* **2000**, *289*, 98.
(11) Schuster, R.; Kirchner, V.; Xia, X. H.; Bittner, A. M.; Ertl, G. *Phys. Rev. Lett.* **1998**, *80*, 5599.
(12) Mandler, D.; Bard, A. J. *Langmuir* **1990**, *6*, 1489.
(13) Mandler, D.; Bard, A. J. *J. Electrochem. Soc.* **1990**, *137*, 2468.
(14) Mandler, D.; Bard, A. J. *J. Electrochem. Soc.* **1989**, *136*, 3143.
(15) Meltzer, S.; Mandler, D. *J. Chem. Soc., Faraday Trans.* **1995**, *91*, 1019.
(16) Grünig, U.; Lehmann, V.; Ottow, S.; Busch, K. *Appl. Phys. Lett.* **1996**, *68*, 747.
(17) Lehmann, V. *J. Electrochem. Soc.* **1993**, *140*, 2836.
(18) Lehmann, V.; Foll, H. *J. Electrochem. Soc.* **1990**, *137*, 653.
(19) Lehmann, V.; Stengl, R.; Luigart, A. *Mater. Sci. Eng., B* **2000**, *69*, 11.
(20) Kleimann, P.; Badel, X.; Linnros, J. *J. Appl. Phys. Lett.* **2005**, *86*, 183108.
(21) Kleimann, P.; Linnros, J.; Juhasz, R. *Appl. Phys. Lett.* **2001**, *79*, 1727.
(22) Avouris, P.; Hertel, T.; Martel, R. *Appl. Phys. Lett.* **1997**, *71*, 285.
(23) Kim, Y.; Choi, I.; Kang, S. K.; Lee, J.; Yi, J. *Appl. Phys. Lett.* **2005**, *86*, 073113.
(24) Kolb, D. M.; Ullmann, R.; Will, T. *Science* **1997**, *275*, 1097.
(25) Xie, Z. X.; Kolb, D. M. *J. Electroanal. Chem.* **2000**, *481*, 177.
(26) Kock, M.; Kirchner, V.; Schuster, R. *Electrochim. Acta* **2003**, *48*, 3213.
(27) Trimmer, A. L.; Hudson, J. L.; Kock, M.; Schuster, R. *Appl. Phys. Lett.* **2003**, *82*, 3327.
(28) Jiang, L. M.; Liu, Z. F.; Tang, J.; Zhang, L.; Shi, K.; Tian, Z. Q.; Liu, K. P.; Sun, L. N.; Tian, Z. W. *J.* Electroanal. Chem. **2005**, *581*, 153.
(29) Shi, K.; Tang, J.; Zhang, L.; Zhou, Y. L.; Qu, D. S.; Sun, L. N.; Tian, Z. Q. *J. Solid State Electrochem.* **2005**, *9*, 398.
(30) Sun, J. J.; Huang, H. G.; Tian, Z. Q.; Xie, L.; Luo, J.; Ye, X. Y.; Zhou, Z. Y.; Xia, S. H.; Tian, Z. W. *Electrochim. Acta* **2001**, *47*, 95.
(31) Tian, Z. W.; Fen, Z. D.; Tian, Z. Q.; Zhuo, X. D.; Mu, J. Q.; Li, C. Z.; Lin, H. S.; Ren, B.; Xie, Z. X.; Hu, W. L. *Faraday Discuss.* **1992**, *94*, 37.
(32) Zu, Y. B.; Xie, L.; Mao, B. W.; Mu, J. Q.; Tian, Z. W. *Electrochim. Acta* **1998**, *43*, 1683.
(33) Zinger, O.; Chauvy, P. F.; Landolt, D. *J. Electrochem. Soc.* **2003**, *150*, B495.
(34) Casalbore, G.; Mastragostino, M.; Valcher, S. *J. Electroanal. Chem.* **1975**, *61*, 33.
(35) Sanchez-Cano, G.; Montiel, V.; Aldaz, A. *Tetrahedron* **1991**, *47*, 877.
(36) Rauwel, F.; Thevenot, D. *Bioelectrochem. Bioenerg.* **1976**, *3*, 284.
(37) Vandeven, J.; Nabben, H. J. P. *J. Electrochem. Soc.* **1991**, *138*, 144.
(38) Bressers, P. M. M. C.; Plakman, M.; Kelly, J. J. *J. Electroanal. Chem.* **1996**, *406*, 131.
(39) Bomchil, G.; Herino, R.; Barla, K.; Pfister, J. C. *J. Electrochem. Soc.* **1983**, *130*, 1611.
(40) Bjorklund, R. B.; Zangooie, S.; Arwin, H. *Langmuir* **1997**, *13*, 1440.
(41) Ohalloran, G. M.; Kuhl, M.; Trimp, P. J.; French, P. *Sens. Actuators, A* **1997**, *61*, 415.
(42) Sotgiu, G.; Schirone, L.; Rallo, F. *Thin Solid Films* **1997**, *297*, 18.